Research Square

Preprints are preliminary reports that have not undergone peer review.
They should not be considered conclusive, used to inform clinical practice,
or referenced by the media as validated information.

Source Time Function Estimation of Earthquakes in the Sarobi Region, Kabul, Afghanistan, Using the Empirical Green's Function Method

Ahmad Baset seadat

basetseadat76@gmail.com

Research Article

Keywords:

Posted Date: November 24th, 2026

DOI: https://doi.org/10.21203/rs.3.rs-11796719/v1

License: This work is licensed under a Creative Commons Attribution 4.0 International License.
Read Full License

Additional Declarations: No competing interests reported.

RESEARCH ARTICLE

SEISMOLOGY • SOURCE-PROCESS STUDIES

Source Time Function Estimation of Earthquakes in the Sarobi Region, Kabul, Afghanistan, Using the Empirical Green's Function Method

Ahmad Basit Seadat

Seismology, Faculty of Science and Nanotechnology, Persian Gulf University, Bushehr, Iran

Corresponding author: Ahmad Basit Seadat | Email: basetseadat76@gmail.com

ARTICLE INFORMATION

Study area	Sarobi region, Kabul, Afghanistan
Study period	2002–2024
Main method	Empirical Green's function (EGF)
Seismic stations	KBL and KBU

Abstract

Source time functions (STFs) of moderate earthquakes in the Sarobi region, east of Kabul, Afghanistan, are extracted using the empirical Green's function (EGF) method. The study builds on a 58-event catalog (2002–2024, M_w 2.51–5.57) whose m_b magnitudes were converted to moment magnitude with the Bormann (2012) relation, $M_w = 1.39 \cdot m_b - 1.94$. Three-component broadband recordings of stations KBL (IU/GSN) and KBU (GE/GEOFON) were retrieved from FDSN web services. Thirteen in-zone targets with $M_w \geq 3.6$ and available data were paired with smaller colocated events ($0.7 \leq \Delta M_w \leq 3.0$, epicentral separation ≤ 12 km), and apparent STFs were obtained by water-level spectral deconvolution in the 0.35–6.5 Hz band, complemented by Brune spectral-ratio fits anchored at $10^{1.5 \cdot \Delta Mw}$, i.e. the theoretical moment ratio of the catalog magnitudes. Six events yielded reliable STFs: apparent source durations (FWHM) of 0.10–0.23 s, trusted corner frequencies of 0.94–2.26 Hz, and Brune stress drops of 1.3–3.3 MPa (mean ≈ 2.1 MPa), within the global 1–10 MPa range for crustal earthquakes. The best-quality solution was obtained for the 19 October 2011 event (M_w 4.04) with a waveform correlation of 0.97 at station KBL. The results are consistent with moderate crustal stress drops and self-similar scaling in the Kabul–Sarobi region.

Keywords: Empirical Green's function; Source time function; Corner frequency; Stress drop; Spectral deconvolution; Sarobi; Kabul; Afghanistan

1. Introduction

Afghanistan lies within the collision zone between the Indian and Eurasian plates, and the continuous convergence of these two plates has produced pervasive and energetic seismicity across the country (e.g., Ambraseys and Bilham, 2003) — from the deep, high-energy events of the Hindu Kush belt in the northeast to the thrust faults and strike-slip systems of the Chaman belt in the south and west (Wheeler et al., 2005). The Kabul region and its eastern margin, including Sarobi district, occupy the transition zone between these structural systems and, in addition to large distant earthquakes, record continuous moderate seismicity with magnitudes usually below 5.5. Knowledge of the source parameters of these moderate seismic-moment events — rupture duration, corner frequency, and stress drop — is of direct importance for seismic hazard assessment, ground-motion modeling, and the monitoring of critical infrastructure along the Kabul–Jalalabad corridor.

The source time function (STF) describes the rate at which seismic moment is released in time; it is the direct basis for estimating the rupture duration and the source complexity and, in combination with the spectral ratio, the corner frequency and the stress drop. In regions such as Afghanistan, where nearby station networks are not always dense and continuous, full waveform inversion or multi-station analysis (e.g., Kikuchi and Kanamori, 1982) is often impractical. Under such conditions, the empirical Green's function (EGF) method — first applied by Hartzell (1978), subsequently by Mueller (1985), and widely used in source-scaling and source-time studies (e.g., Dreger, 1994) — provides an economical and reliable solution: the recording of a smaller, nearby event is used as the true Green's function instead of a theoretical path model, and in the ratio of the two recordings the path, instrument, and site effects cancel, leaving the "signature" of the source.

This article is the second stage of a continuing research program on the seismicity of the Sarobi region. In the first stage of the program, the m_b magnitudes of the 58-event catalog for the period 2002–2024 were converted to moment magnitude M_w with the Bormann relation — a step that is essential for consistent estimates of the seismic moment and of the magnitude differences of the event pairs. In the second stage, which is the subject of the present paper, broadband waveforms from the two nearby stations KBL and KBU were retrieved from the FDSN web services, paired for the target events, and processed by water-level spectral deconvolution to extract the source time function; the source parameters, including the apparent duration, corner frequency, source radius, and Brune stress drop, were

then estimated. Section 2 introduces the data and the magnitude conversion; Sections 3 and 4 describe the analysis and the processing; Section 5 presents the results for the six reliable events; and Sections 6 and 7 are devoted to the discussion, the limitations, and the conclusions.

1.1. Novelty and the difference between the present study and previous work

In recent years, various studies have addressed the earthquakes and the active faults of Kabul and its surroundings. Most of these studies have focused on fault identification, the geological structure, and seismic hazard assessment. Information on how the earthquake sources rupture and on their physical characteristics in the Sarobi region — particularly for small and moderate earthquakes — nevertheless remains limited.

In the present study, an attempt is made to investigate the source characteristics of the earthquakes of the Sarobi region using the empirical Green's function (EGF) method. To this end, the recordings of seismic stations were used, and waveform analysis was employed to estimate the source time function, the rupture duration, the corner frequency, and the stress drop.

The difference between this study and many previous investigations is that, instead of focusing solely on fault identification and seismic hazard, it examines the behavior of the earthquake source itself. The results provide preliminary information on the source characteristics of the earthquakes of the Sarobi region and lay the groundwork for future research on earthquake behavior and on the seismic properties of the Kabul region.

1.2. Study region

The study region is located in Sarobi district at the eastern margin of Kabul province, within the rectangular selection window of 34.30–34.65°N and 69.30–69.75°E that was used for the target events (Section 2.1). The area lies in the transition zone between the deep, energetic seismicity of the Hindu Kush belt to the northeast and the thrust and strike-slip systems of the Chaman belt to the south and west, and it records continuous moderate seismicity with magnitudes usually below 5.5 (Section 1). Figure 1 shows a satellite view of the district together with the approximate north–south surface trend of the Sarobi fault.

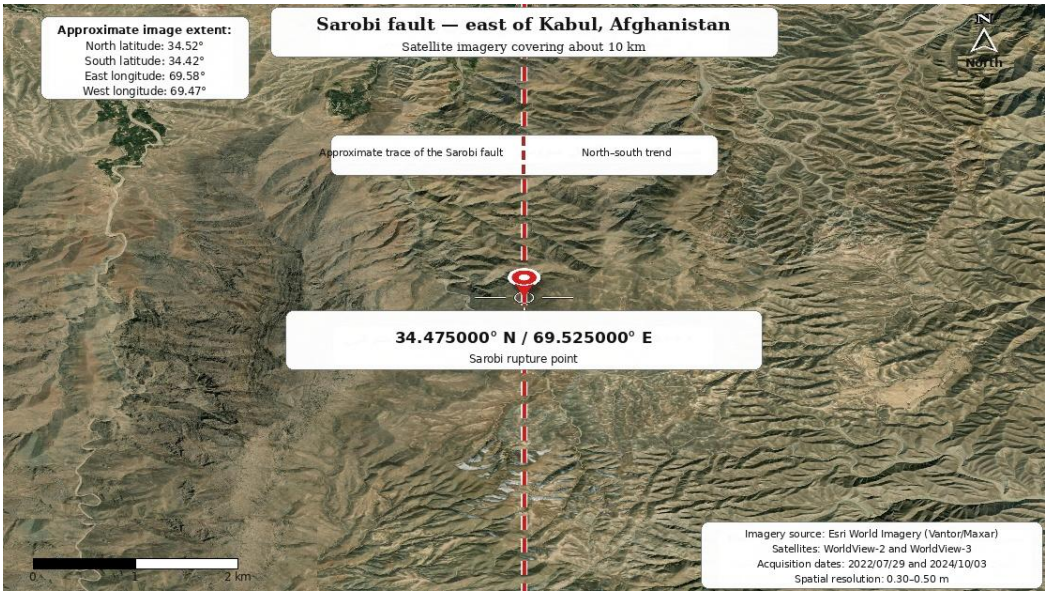

Figure 1. Satellite view of Sarobi district, east of Kabul, Afghanistan, with the approximate north–south trace of the Sarobi fault (red dashed line) and the reference coordinates 34°37′47.0″N, 69°52′58.0″E. Base imagery: Esri World Imagery (Vantor/Maxar), WorldView-2 and WorldView-3, acquired on 6 October 2020 and 18 June 2021.

2. Data and seismic catalog

2.1. Research catalog and conversion of m_b to M_w

The research catalog comprises 58 seismic events of the period 2002–2024, all identified by official ISC event IDs; 53 events have the ISC as their magnitude-reporting agency, two events come from the national network (NNC), and the remainder are from NEIC, IDC, and NDI. Of these, 29 events are recorded in the "in-zone events" worksheet of the catalog and lie within the rectangular window of latitude 34.30–34.65°N and longitude 69.30–69.75°E, which forms the basis for the selection of the target events in this study. An overview of the catalog — the spatial distribution, the magnitude–time distribution, and the depth distribution — is given in Figure 2. After conversion, the magnitudes range from M_w 2.51 to 5.57, and the majority of the events fall in the range M_w 2.9–4.0.

Because the original catalog reported only m_b magnitudes, whereas estimating the seismic moment (Hanks and Kanamori, 1979) and the magnitude differences of the EGF pairs requires moment magnitude — for which empirical conversion relations from m_b are available (e.g., Scordilis, 2006) — all m_b values were converted to M_w using the orthogonal regression (OSR) relation of Bormann (2012), recorded as Eq. (3.118) in Chapter 3 of the NMSOP-2 manual:

$$M_w = 1.39 \cdot m_b - 1.94$$

This relation was calibrated on 480 events with a standard deviation of ±0.33 and is valid for reference m_b values between 4.5 and 7.5; since the m_b values of the research catalog range from 3.2 to 5.4, its application to values below 4.5 is in fact an extrapolation and carries a larger uncertainty — a caveat that is also documented in the "method and control" worksheet of the catalog file. The conversions were performed with ROUND_HALF_UP decimal rounding to two decimal places, and only one event with an M_L magnitude (ID 636673972) was left unchanged. In total, 86 rows in the two event worksheets (29 rows of the in-zone sheet and 57 of the 58 rows of the full sheet) were updated, and the correctness of the operation was verified cell by cell against the 178 changed cells (86 magnitudes, 86 magnitude types, and 6 documentation cells). These M_w values form the moment anchor of the spectral ratio in Section 3.3.

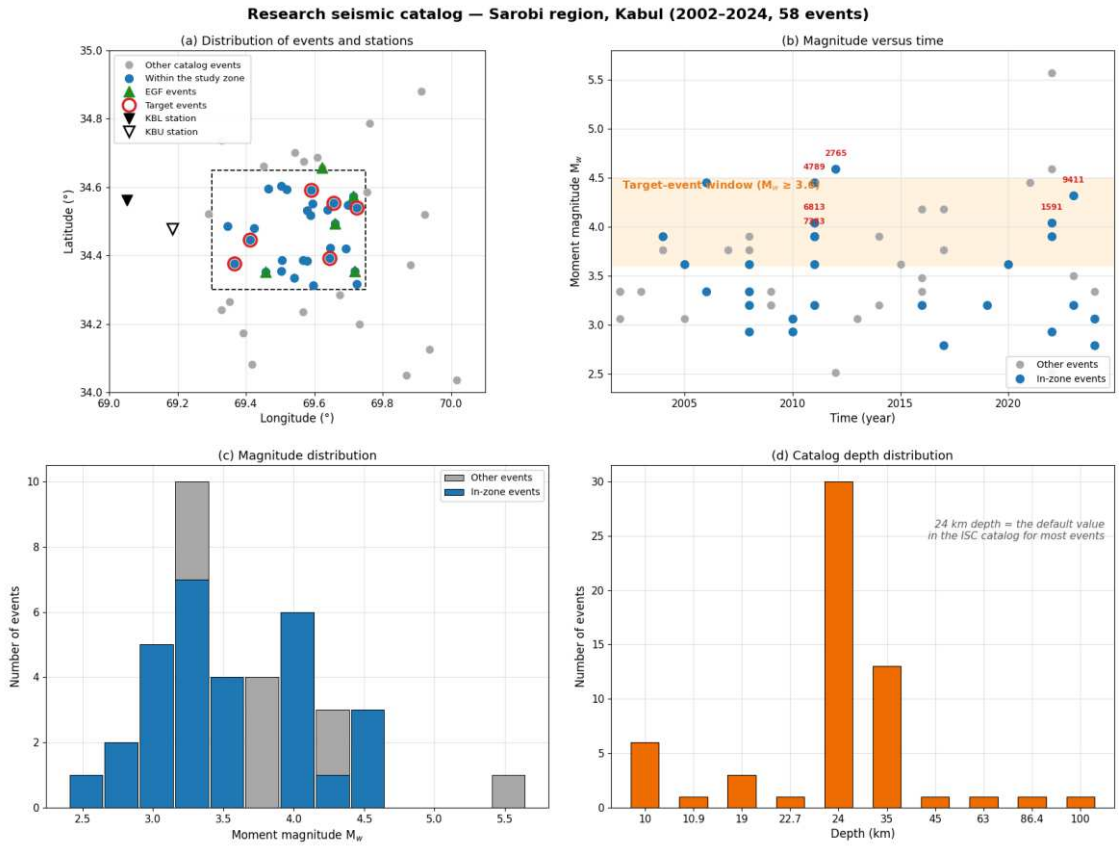

Figure 2. Overview of the 58-event Sarobi catalog (2002–2024): (a) map of the events and the broadband stations; (b) magnitude versus time; (c) magnitude distribution; and (d) depth distribution. The dashed rectangle shows the study window.

As can be seen in Figure 2d, 30 events are reported at the fixed depth of 24 km, 13 events at 35 km, and 6 events at 10 km — a pattern indicating that part of the depths are a

priori defaults of routine cataloging procedures rather than accurate canonical estimates. This point must be taken into account both in interpreting the pair geometry and in picking the phase arrivals (Section 4).

2.2. Broadband stations

Two broadband stations within 70 km of the study window provide continuous data: station KBL of the Global Seismographic Network (GSN; network IU) in Kabul and station KBU of the GEOFON network (network GE). The characteristics of both stations are given in Table 1. The epicentral distances of the in-zone events range from 28.4 to 67.2 km to KBL and from 19.6 to 58.3 km to KBU; at these distances, recording events with $M_w \geq 2.5$ with a sufficient signal-to-noise ratio in the analyzed band is feasible.

Table 1. Characteristics of the broadband stations used.

Station	Network	Latitude (°N)	Longitude (°E)	Sensor	Operating period	Events with data
KBL	IU (GSN)	34.5408	69.0432	STS-2/VBB	2006-11 to 2024-01	23
KBU	GE (GEOFON)	34.5151	69.1347	STS-2/N	2005-11 to 2026-11	9

Number of events with data out of the 29 in-zone events; four events were recorded at both stations.

2.3. Waveform availability and supplementary events

Data availability was assessed by trial downloads of 80-s windows around the origin time of each of the 29 in-zone events from the dataselect web services of EarthScope Consortium (formerly IRIS; EarthScope Consortium, 2026) and GEOFON. KBL has complete data for 23 events and KBU for 9 events; four events were recorded at both stations, and the union of the two stations covers 28 of the 29 in-zone events — the only exception is the event of 10 March 2004, which predates the installation of both stations and has no recordings. The three-component waveforms (BHE, BHN, BHZ) of the required events were then downloaded for the analysis.

So that the pool of EGF candidates would not be restricted to the research catalog, the USGS and GEOFON catalogs were also queried around each target event (a window of ±0.15°, for events smaller than the target by at least 0.7 magnitude units; U.S. Geological Survey, 2026). After removal of duplicates, six supplementary events were added to the pool; their m_b magnitudes were also converted to M_w with the same Bormann relation to preserve

consistency with the research catalog. Finally, each target event was paired with the best qualified candidates from both sources (Section 3.1).

3. Analysis method

3.1. Principle of the empirical Green's function and pair selection

If two events occur close enough to one another, their recordings at a common station can be written as

$$U_1(\omega) = S_1(\omega) \cdot P(\omega) \cdot I(\omega) + N_1(\omega) \quad (1)$$

where S is the source spectrum, P the path response (focusing, attenuation, and scattering), I the instrument response, and N the noise. Because the smaller (EGF) event occurs at nearly the same hypocentral distance, P and I are practically identical for the two events and cancel in the spectral ratio; if the small event behaves as a point source (a short pulse), the spectral ratio directly displays the ratio of the two source spectra. To ensure this assumption, the EGF candidates were selected with the customary criteria (Mueller, 1985): a moment-magnitude difference of at least 0.7 and at most 3.0 (maximum score at $\Delta M_w \approx 1.5$), an epicentral separation of at most 12 km, a depth difference of at most 25 km, and recording at the same station. The pairs were scored on the closeness of the magnitude difference to 1.5 and on the smallness of the separation, and up to six top candidates were retained for each target event. The overall scheme of the method is illustrated in Figure 3.

The target events were the in-zone events with $M_w \geq 3.6$ and available station recordings: 14 events, one of which (10 March 2004) has no recorded data, so that 13 events proceeded to the pairing and processing stage. Table 3 in Section 5.1 lists these 13 events together with the final outcome for each of them.

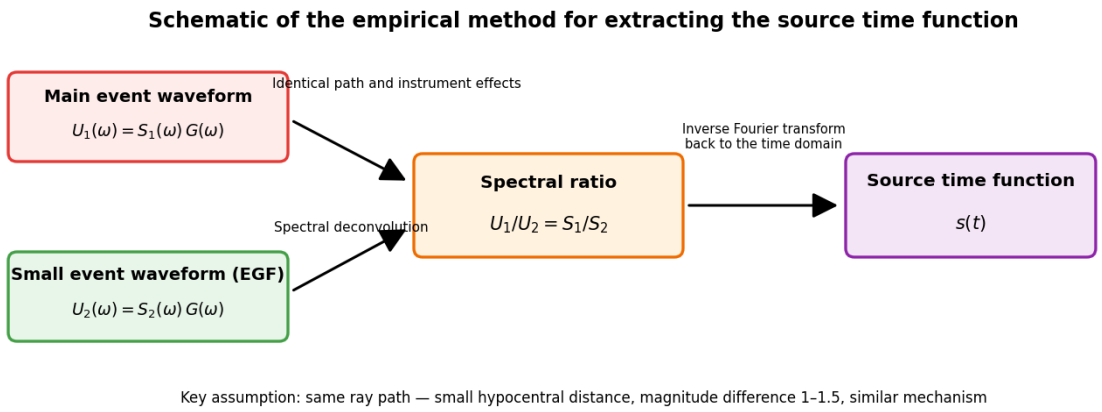

Figure 3. Schematic of the empirical Green's function method: in the spectral ratio/deconvolution of two nearby recordings, the path and instrument effects cancel and the source time function, the corner frequency, and the stress drop are recovered.

3.2. Water-level spectral deconvolution

The apparent source time function is obtained by spectral deconvolution of the main-event recording by the EGF recording in the frequency domain. To avoid instability at frequencies where the EGF spectrum is weak, the standard water-level solution was used:

$$D(\omega) = \frac{U_1(\omega) \cdot U_2^*(\omega)}{|U_2(\omega)|^2 + \lambda^2}, \quad \lambda = 0.08 \cdot max\,|U_2(\omega)| \tag{2}$$

After band-limiting (a band-pass of 0.35–6.5 Hz with a cosine ramp up to 7 Hz), the deconvolution output is transformed back to the time domain with an inverse Fourier transform, yielding the apparent source time function, which is then smoothed with a 0.1-s moving average. The deconvolution noise floor is computed by repeating the same operation on two pre-arrival noise segments of the two events and is plotted in the figures as the detectability limit of the STF. The parameters extracted from each STF are the full width at half maximum (FWHM), the width at the 20% level of the peak (τ_{20}), the peak time, and the area under the curve (proportional to the moment ratio of the two events).

3.3. Spectral ratio, corner frequency, and source parameters

The amplitude spectra of the two windows are smoothed with the Konno–Ohmachi (1998) smoothing (bandwidth parameter 40), and only frequencies with a signal-to-noise ratio above 3 for both events participate in the fits. The spectral-ratio model is a special case of the ω-square source model of Brune (1970, 1971):

$$| U_1(f) / U_2(f) | = \Omega_{0r} \cdot \frac{1 + (\frac{f}{f_{c,EGF}})^2}{1 + (\frac{f}{f_{c,target}})^2} \quad (3)$$

Experiments showed that fitting the level and the corner frequency simultaneously is unstable when the corner of the EGF spectrum does not fall within the reliable band; in all pairs of this study the EGF spectral corner was constrained above 25 Hz (beyond the deconvolution band). The target corner frequency was therefore fitted with the low-frequency level of the ratio anchored to the theoretical moment ratio of the catalog magnitudes, namely $10^{1.5 \cdot \Delta Mw}$; this choice is justified by the fact that, at low frequencies, the path and instrument effects cancel in the ratio and the remaining level is directly the moment ratio of the two events. The source parameters were then computed from the standard Brune relations with a shear-wave velocity of β = 3.5 km/s:

$$M_0 = 10^{1.5M_w+9.1}\, N \cdot m, \quad r = \frac{2.34\beta}{2\pi f_c}, \quad \Delta\sigma = \frac{7M_0}{16r^3} \quad (4)$$

Because the stress drop varies with the inverse third power of the corner frequency, a small error in f_c leads to a large error in Δσ. The quality of the corner-frequency fit is therefore reported with an RMS grading (grade A for RMS ≤ 0.25 and grade B for RMS ≤ 0.45), and the radius and the stress drop are calculated only for corner frequencies within the band (0.4–13 Hz) that carry a trusted grade. In addition, six pair-level quality-control criteria (Table 2) were applied for the acceptance of each pair.

Table 2. The six quality-control criteria applied to the EGF pairs.

Criterion	Acceptance threshold	Description
Window correlation	cc ≥ 0.45	Maximum correlation of the full window and of the onset pulse after alignment
STF peak position	0.05–3.0 s	The peak must not fall in the noise or far from the arrival time
Corner frequency in band	0.4–13 Hz	f_c must lie effectively within the band, and $f_{c,EGF}$ must be substantially higher than the target f_c
Low-frequency flatness of the ratio	deviation ≤ 0.25 dex	Stability of the ratio level in the 0.5–1.5 Hz band
Moment consistency	$\lvert\log_{10}(\Omega_{0r}) - 1.5 \cdot \Delta M_w\rvert \le 0.8$	The spectral-ratio level must be consistent with the moment anchor of the catalog magnitudes
Signal-to-noise ratio	target ≥ 5, EGF ≥ 4	Mean SNR in the 0.4–8 Hz band

A pair that passes all six criteria is “fully accepted”, and a pair that passes five criteria is “accepted with caution”.

4. Waveform processing

The processing chain was run identically for each pair and for both the P and the S band. First, the waveforms are corrected to velocity using the station instrument response (the StationXML applicable to the time of each event); the pre-filter of the response removal is set at 0.3–0.6 Hz and 19.2–22.4 Hz with a water level of 60. A zero-phase Butterworth band-pass of 0.4–16 Hz with four corners is then applied with exactly the same settings for both events. The horizontal components are rotated into radial (R) and transverse (T) components using the station-to-event azimuth. The P arrival is picked on the Z component (or on R in its absence) and the S arrival on the stronger horizontal component, with a short-term/long-term-average (STA/LTA) ratio detector anchored on the theoretical iasp91 arrival times. The two events are aligned by maximizing the cross-correlation in the deconvolution band (0.4–7 Hz) within a ±3-s window at 25-ms steps, and the alignment is then fine-tuned on the onset pulse (a 1.6-s window). The final deconvolution is performed on a 5-s P window (starting 0.5 s before the arrival) and a 9-s S window with an 8% cosine taper on the trailing edge.

Two practical lessons emerged from the processing that are valuable for future applications in this region. First, because a large fraction of the catalog depths are default values, the theoretical iasp91 times differed from the actual phase arrivals by up to about 3 s; the final picking was therefore performed in a data-driven manner, with STA/LTA in a limited window around the theoretical anchor, instead of using the theoretical times directly. Second, in the common implementation of the classic_sta_lta function the function value is zero at the beginning of the window (until the LTA fills), which can miss the true P onset; the search window was therefore cut back by the LTA length to remove this problem. After the deconvolution, each band was evaluated against the six criteria of Table 2, and for each target event the band with the highest score (the number of accepted criteria, and then the correlation) was selected as the final result.

5. Results

5.1. Pairing and quality-control outcome

Of the 13 processed target events, 6 events yielded reliable source time functions; 3 events had candidates but were rejected by the quality-control criteria (mainly because of a

low window correlation or a corner frequency outside the band), and 4 events had no qualified candidate within the 12-km radius and the magnitude-difference range. Table 3 lists the full set of 13 events and the fate of each; all accepted events had been recorded at station KBL.

Table 3. The 13 target events and the outcome of the pairing and processing.

Target event	Date	M_w	EGF	ΔM_w	Distance (km)	Station	Outcome
8011815	2005-12-27	3.62	—	—	—	—	No qualified candidate
8079421	2006-01-27	4.45	—	—	—	—	Rejected at quality control
13393824	2008-09-08	3.62	—	—	—	—	Rejected at quality control
16587344	2011-06-01	3.62	—	—	—	—	No qualified candidate
16577383	2011-06-04	3.90	14876428	0.84	8.9	KBL	Accepted (5/6)
16557032	2011-06-04	3.90	—	—	—	—	No qualified candidate
17324789	2011-09-25	4.45	14876428	1.39	11.2	KBL	Accepted (4/6)
17386813	2011-10-19	4.04	13335548	0.70	4.0	KBL	Accepted (6/6)
601022765	2012-05-18	4.59	608498978	1.39	8.0	KBL	Accepted (6/6)
618936064	2020-08-30	3.62	—	—	—	—	No qualified candidate
624605874	2022-07-16	3.90	—	—	—	—	Rejected at quality control
625391591	2022-12-11	4.04	604093297	0.84	8.0	KBL	Accepted (5/6)
626329411	2023-06-25	4.32	610415472	1.53	6.6	KBL	Accepted (5/6)

Distance is the epicentral separation between the target and the EGF event; ΔM_w is the catalog moment-magnitude difference. The event of 10 March 2004 (M_w 3.90) predates the installation of the stations and is not among the processed targets.

5.2. Source time function and source parameters

Table 4 summarizes the geometry of the six accepted pairs and their source time function parameters, and Table 5 shows the estimated source parameters (seismic moment, corner frequency, radius, and Brune stress drop). The full width at half maximum of the source duration lies between 0.103 and 0.227 s and, as expected, the larger events have longer durations and lower corner frequencies. The trusted corner frequencies of four events range from 0.94 to 2.26 Hz, and the corresponding Brune stress drops are 1.3–3.3 MPa (mean ≈ 2.1 MPa).

Table 4. Geometry of the accepted pairs and their source time function parameters.

Target event	M_w	EGF	M_w (EGF)	ΔM_w	Distance (km)	Station	Band	τ_{FWHM} (s)	τ_{20} (s)	cc
601022765	4.59	608498978	3.20	1.39	8.0	KBL	P	0.128	0.325	0.60
17324789	4.45	14876428	3.06	1.39	11.2	KBL	S	0.156	0.250	0.69
626329411	4.32	610415472	2.79	1.53	6.6	KBL	P	0.227	0.450	0.57

Target event	M_w	EGF	M_w (EGF)	ΔM_w	Distance (km)	Station	Band	τ_{FWHM} (s)	τ_{20} (s)	cc
17386813	4.04	13335548	3.34	0.70	4.0	KBL	P	0.205	0.300	0.97
625391591	4.04	604093297	3.20	0.84	8.0	KBL	P	0.116	0.125	0.76
16577383	3.90	14876428	3.06	0.84	8.9	KBL	P	0.103	0.150	0.67

Band: wave used for the deconvolution; τ_{20}: width of the STF at 20% of the peak; cc: window correlation after alignment.

Table 5. Estimated source parameters (Brune model, β = 3.5 km/s).

Target event	M_w	M_0 (N·m)	Band of f_c	f_c (Hz)	Grade	f_c (EGF) (Hz)	$1/(2\pi f_c)$ (s)	r (m)	$\Delta\sigma$ (MPa)	QC
601022765	4.59	9.66×10^{15}	S	0.94	A	≥ 25	0.170	1393	1.6	6/6
17324789	4.45	5.96×10^{15}	S	0.40	—	≥ 25	0.398	—	—	4/6
626329411	4.32	3.80×10^{15}	P	1.20	B	≥ 25	0.133	1085	1.3	5/6
17386813	4.04	1.45×10^{15}	P	2.26	B	≥ 25	0.070	577	3.3	6/6
625391591	4.04	1.45×10^{15}	P	2.00	B	≥ 25	0.079	650	2.3	5/6
16577383	3.90	8.91×10^{14}	S	2.41	—	≥ 25	0.066	—	—	5/6

The corner-frequency grade is based on the fit RMS (A: ≤ 0.25; B: ≤ 0.45); the radius and the stress drop are computed only for trusted corner frequencies. M_0 follows from the catalog M_w (Eq. 4).

5.3. Selected events

This section reviews the results of the six events one by one. Each figure has four panels: (a) the aligned waveforms of the two events; (b) the apparent source time function with the deconvolution noise floor and the FWHM width; (c) the Konno–Ohmachi smoothed spectra together with the noise; and (d) the spectral ratio with the Brune fit (the anchored level and the free fit).

The highest-quality result belongs to the event of 19 October 2011 (ID 17386813, M_w 4.04), which was processed with the EGF event 13335548 at a separation of 4 km and reached a pulse correlation of 0.971; all six quality criteria were passed. The STF pulse is legible and clearly separated from the noise, its FWHM duration is 0.205 s, its corner frequency is 2.26 Hz (grade B), and its Brune stress drop is 3.3 MPa (Figure 4).

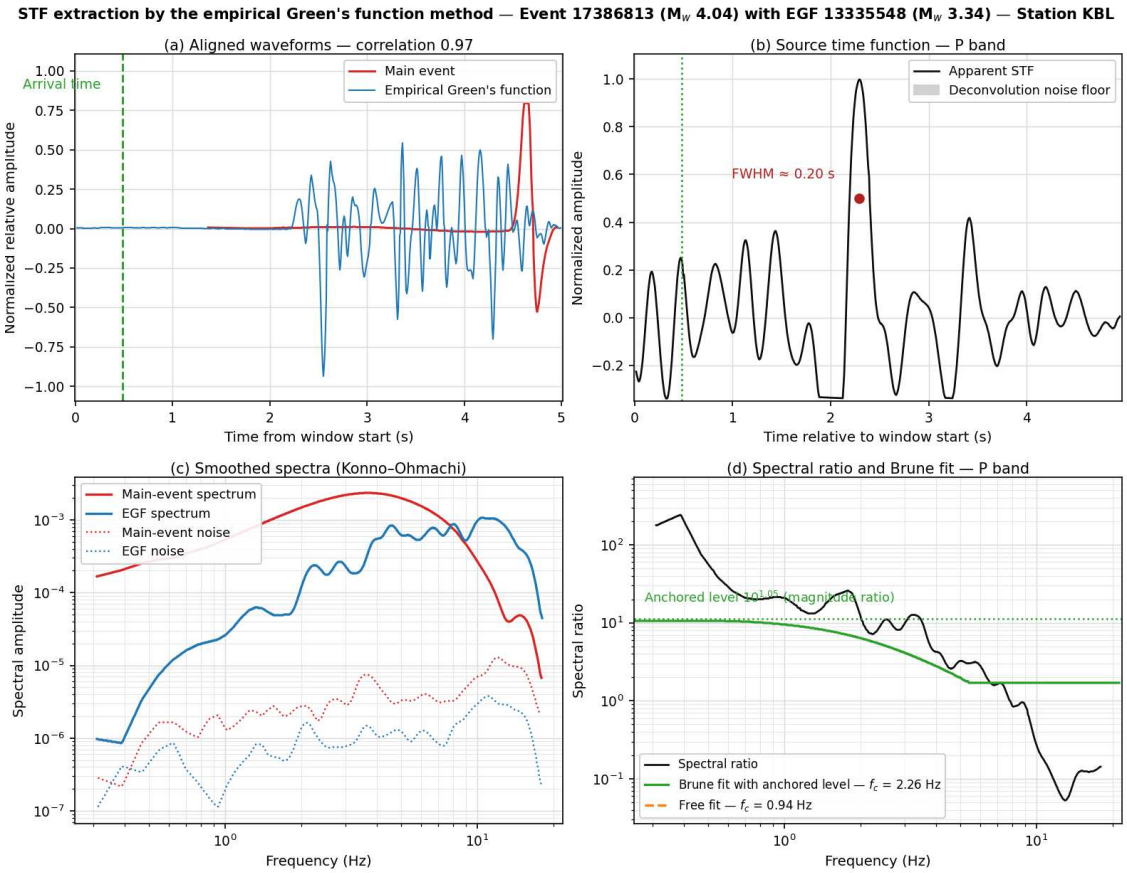

Figure 4. Event 17386813 (M_w 4.04) with EGF event 13335548 at station KBL — the highest-quality pair of the study (cc = 0.97).

The event of 18 May 2012 (ID 601022765, M_w 4.59) is the largest event analyzed and, like the previous one, passed all six criteria. Its corner frequency was fitted with the highest confidence (grade A) at 0.94 Hz, giving a stress drop of 1.6 MPa and a duration of 0.128 s (Figure 5); in the f_c–M_w diagram, this event falls exactly on the 1-MPa stress-drop contour (Figure 10b).

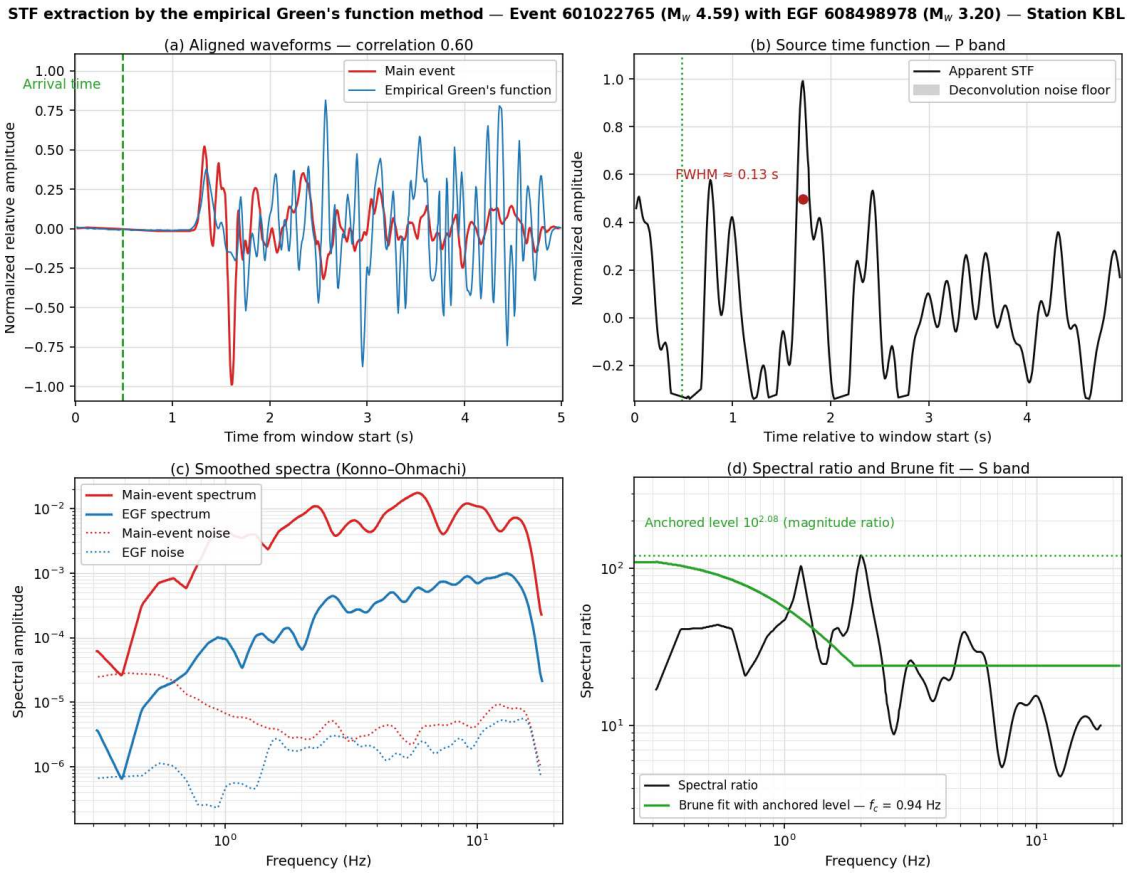

Figure 5. Event 601022765 (M_w 4.59) with EGF event 608498978 — the largest analyzable event, with grade A.

The event of 25 September 2011 (ID 17324789, M_w 4.45) is the example analyzed in the S-wave band: the correlation is 0.685 and the FWHM duration is 0.156 s, but the fitted corner frequency (0.40 Hz with an RMS of 0.607) is unreliable, and no radius or stress drop is reported for it (Figure 6). The value of this example lies in demonstrating the resolution power of the S band for the duration, even when the corner-frequency fit is unsuccessful.

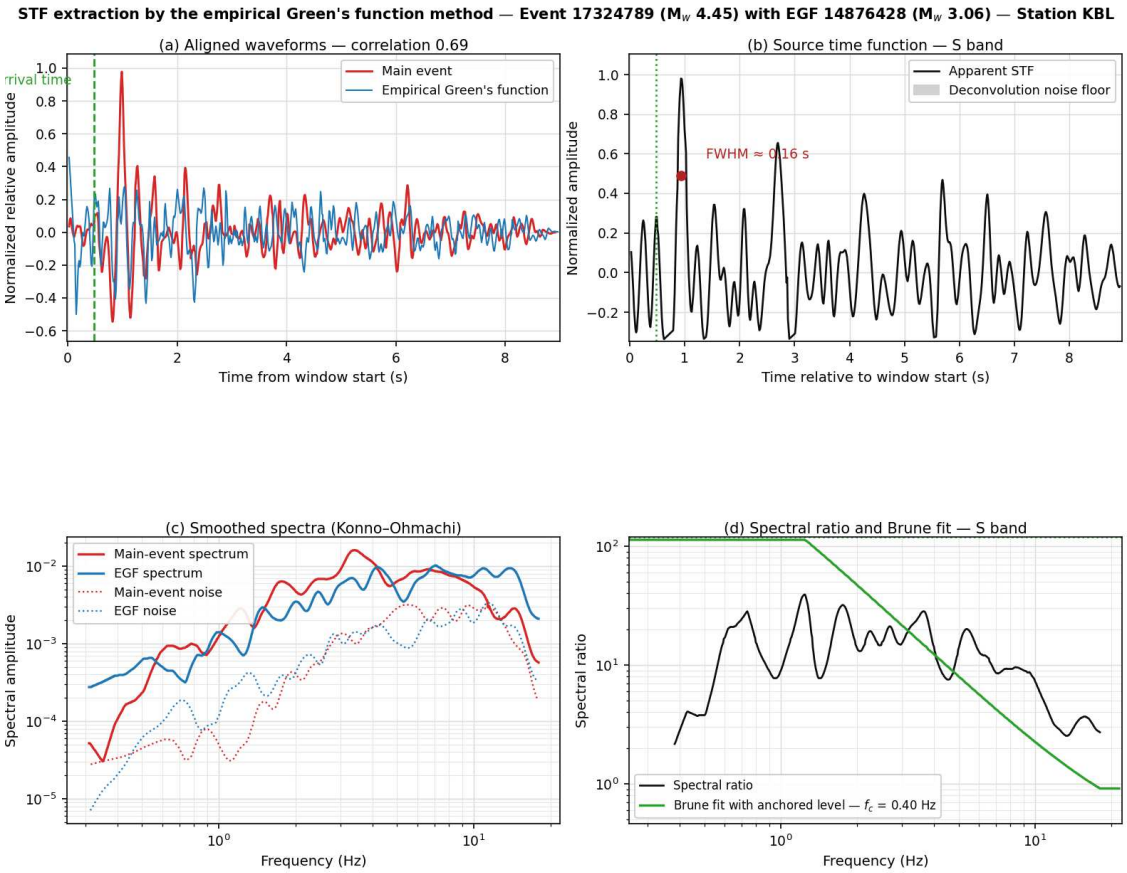

Figure 6. Event 17324789 (M_w 4.45) with EGF event 14876428 — analysis in the S-wave band.

The event of 25 June 2023 (ID 626329411, M_w 4.32) was processed with the largest magnitude difference (ΔM_w = 1.53) and a smaller EGF (M_w 2.79); the longest FWHM duration (0.227 s), a corner frequency of 1.20 Hz (grade B), and a stress drop of 1.3 MPa — the lowest value among the pairs — were obtained (Figure 7).

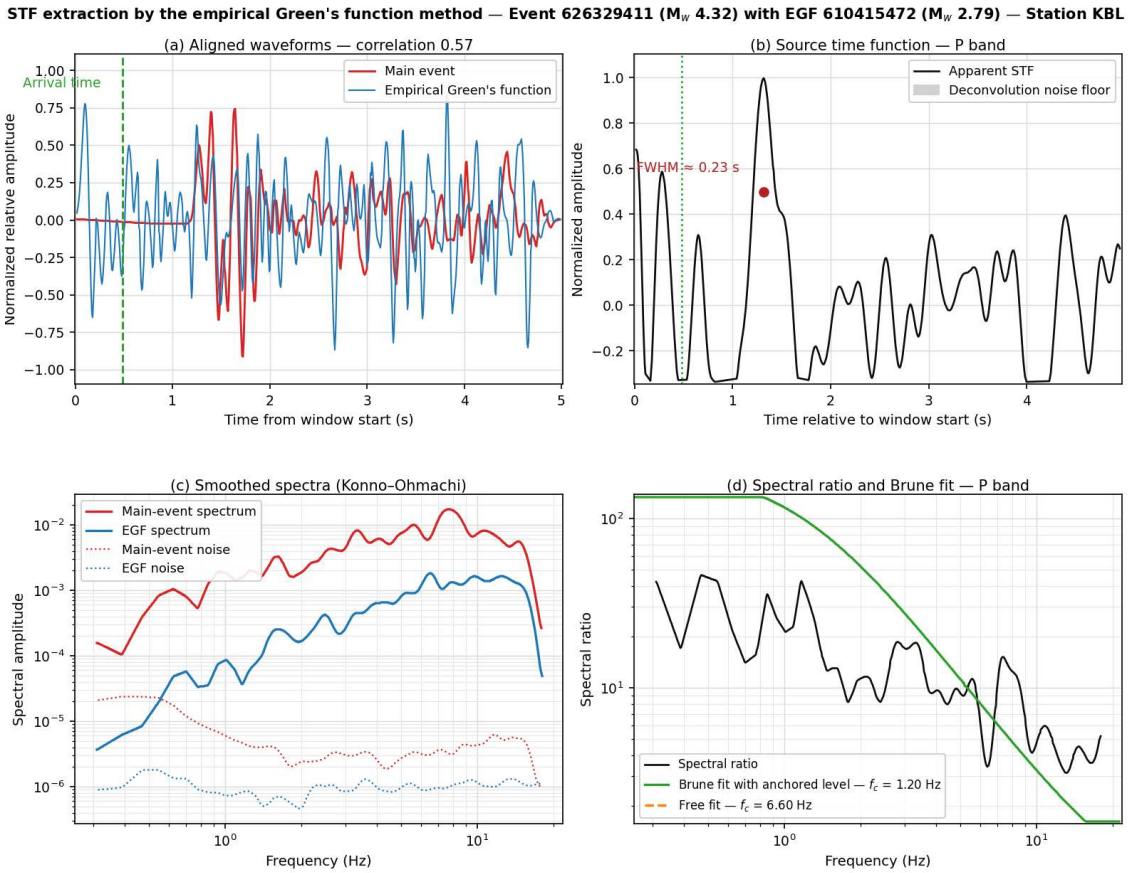

Figure 7. Event 626329411 (M_w 4.32) with EGF event 610415472 — the largest magnitude difference (ΔM_w = 1.53).

The event of 11 December 2022 (ID 625391591, M_w 4.04) has a duration of 0.116 s, a corner frequency of 2.00 Hz, and a stress drop of 2.3 MPa (Figure 8).

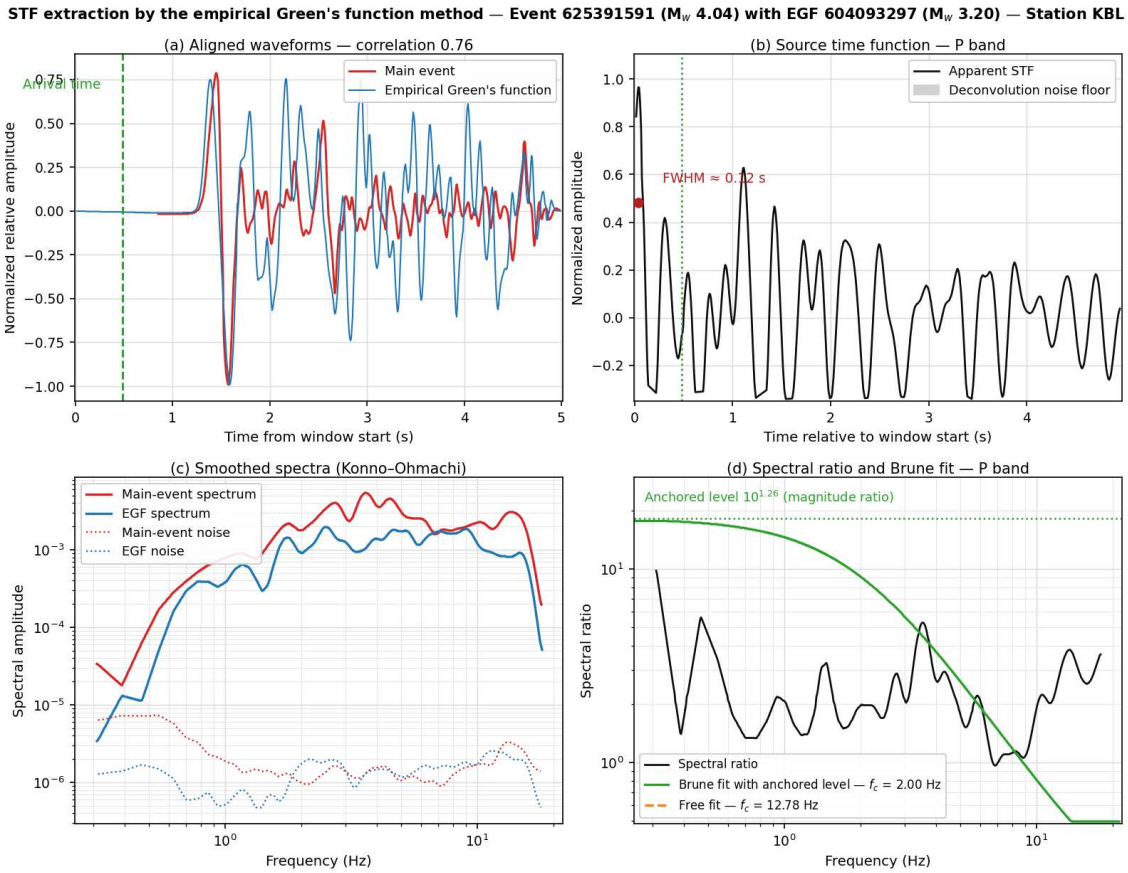

Figure 8. Event 625391591 (M_w 4.04) with EGF event 604093297 at station KBL.

The event of 4 June 2011 (ID 16577383, M_w 3.90), with a duration of 0.103 s, is the smallest member of the set; its corner frequency fell at the confidence boundary and its stress drop was not reported (Figure 9).

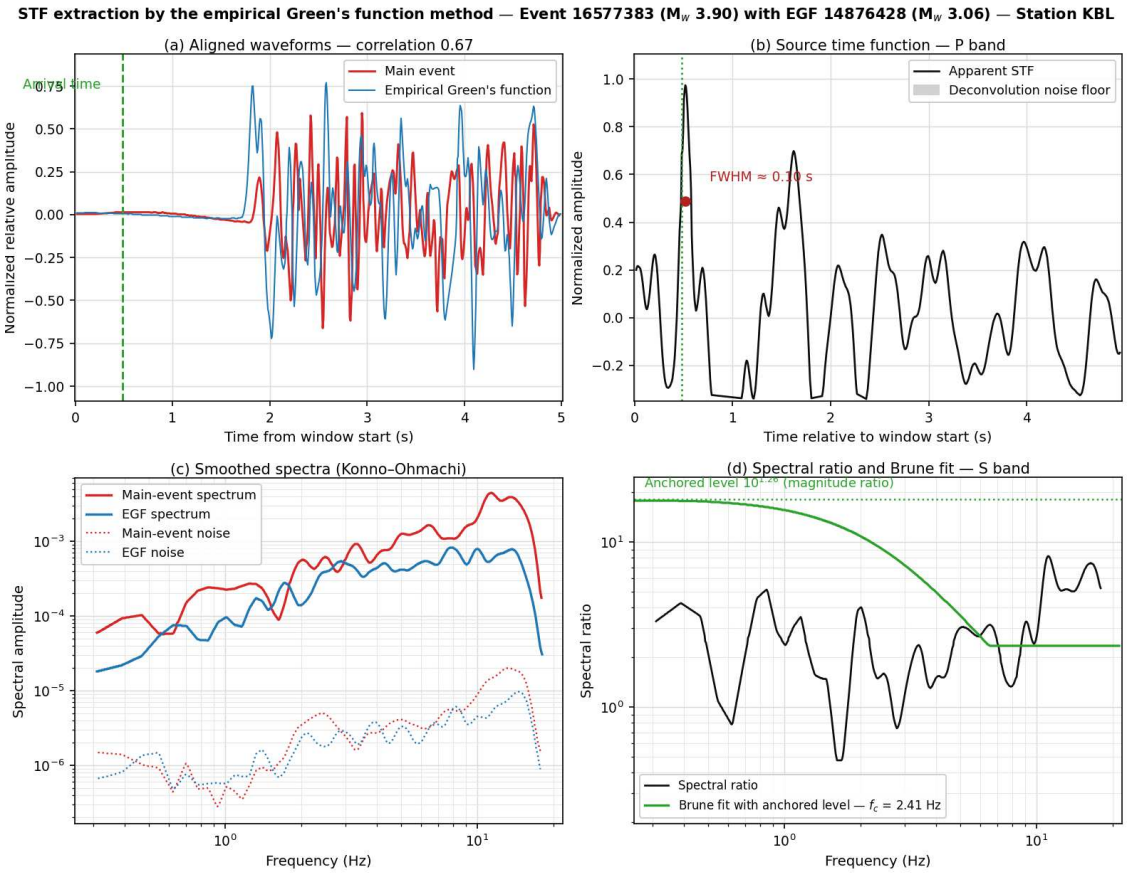

Figure 9. Event 16577383 (M_w 3.90) with EGF event 14876428 — the smallest accepted event.

5.4. Regional synthesis

Figure 10 shows the regional summary of the results: in the corner-frequency-versus-magnitude plot, the four events with a trusted grade fall within the field of the 1–10 MPa stress-drop contours, and the slope of their scaling is consistent with self-similarity (an approximately constant stress drop); the comparison of the FWHM durations with the Brune scale $1/(2\pi f_c)$ likewise shows the consistency of the two independent duration estimates. The distribution of the estimated stress drops (1.3–3.3 MPa) is centered on a mean value of ≈ 2.1 MPa — a pattern that is common for moderate crustal earthquakes in active thrust belts.

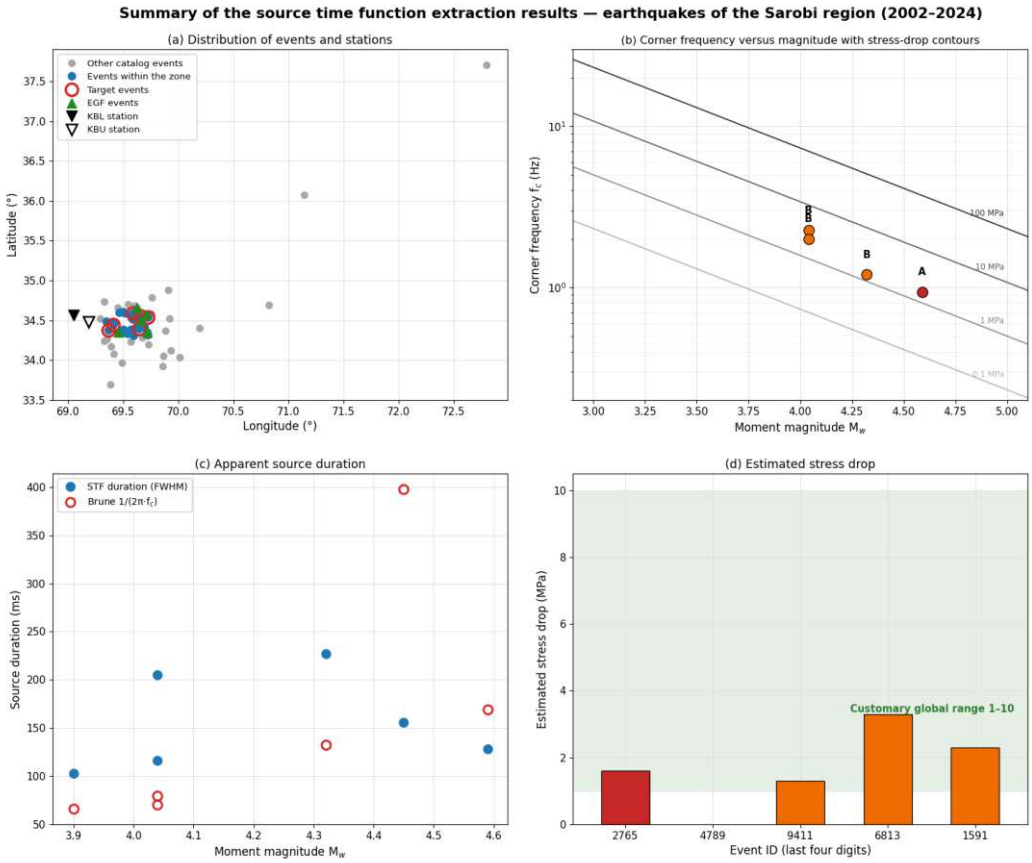

Figure 10. Summary of the results: (a) distribution of the target and EGF events and of the stations; (b) corner frequency versus M_w with stress-drop contours; (c) apparent source duration; and (d) estimated stress drop.

6. Discussion

The estimated stress drops (1.3–3.3 MPa for the four events with a trusted grade) fall within the customary global range of 1–10 MPa for crustal earthquakes, and their scatter is consistent with a self-similar picture. The absence of abrupt trends in the f_c–M_w plot and the consistency of the FWHM durations with $1/(2\pi f_c)$ support the results internally; nevertheless, the four-event sample is not sufficient for firm regional conclusions, and these figures should be regarded as the first estimates of the source parameters of the Sarobi region.

The main limitations of the analysis should be stated explicitly. First, the deconvolution band is capped at 7 Hz; durations close to 0.10 s approach this limit and should be regarded as upper bounds on the resolvable values. Second, the spectral corner of the EGF was not seen within the band in any pair (the EGF corner was constrained above 25 Hz); the point-like character of the EGF was therefore not a direct observation of the spectral corner but followed from the magnitude difference of at least one unit and from the appropriate shape

of the ratio at low frequencies. Third, the fixed 24-km depths of the catalog affect both the pair geometry and the phase picking; the timing error of up to about 3 s was compensated in the data-driven picking stage, but the true depth difference within the pairs remains unknown. Fourth, the moment anchor of the spectral ratio comes from the converted catalog magnitudes; an uncertainty of ±0.3 in M_w can shift M_0, and with it the stress drop, by roughly a factor of two. Fifth, all results were obtained at the single station KBL; the fitted f_c is therefore an "apparent corner frequency" at the station path, and neither the directivity effect nor the site effect of the station has been averaged out.

7. Conclusions and recommendations

This research showed that source time function extraction with data from a single local broadband station is feasible and valid for the moderate earthquakes of the Sarobi region, provided that a smaller neighboring event exists (a magnitude difference of 0.7–3 and an epicentral separation of less than 12 km) and that the quality-control criteria are applied rigorously. Of the 13 target events, six events of the period 2011–2023 have reliable source time functions: apparent durations of 0.10–0.23 s, trusted corner frequencies of 0.94–2.26 Hz, and Brune stress drops of 1.3–3.3 MPa — results that are consistent with self-similar scaling and with the moderate crustal stress drops of the region. The first step of the same program — the uniform conversion of the m_b magnitudes to M_w with the Bormann relation — played a key role in the moment anchor of the spectral ratio, and its correctness was verified cell by cell.

Four recommendations are put forward to complete this effort. First, the source time function of each event should be computed from several independent EGF pairs and the results combined by weighted averaging to reduce the directivity effect. Second, the events should be relocated precisely — with particular attention to the depth — before pairing, using local catalog data. Third, cut-and-paste (CAP) waveform inversion should be applied to the larger events of the catalog with a regional velocity model, which constrains the mechanism and the depth simultaneously. Fourth, data from neighboring stations should be used for the period 2005–2006, during which KBL has no data, and to complete the rejected pairs. The continued recording of station KBU after the discontinuation of KBL is likewise of strategic importance for the future monitoring of the seismicity of Sarobi.

Declarations

Ethics approval and consent to participate

Not applicable.

Consent for publication

Not applicable.

Availability of data and material

The earthquake catalogue data are identified by the International Seismological Centre (ISC) event IDs. The waveform data used in this study are available through the EarthScope FDSN web services and GEOFON. The processed data supporting the findings of this study are available from the corresponding author upon reasonable request.

Competing interests

The author declares that there are no competing interests.

Funding

Not applicable. No specific funding was received for this research.

Authors' contributions

ABS conceived and designed the study, collected and processed the data, performed the analysis, prepared the figures and tables, and wrote and revised the manuscript. The author read and approved the final manuscript.

Acknowledgements

Not applicable.

References

Ambraseys, N. N., & Bilham, R. (2003). Earthquakes and Afghanistan deformation. Geophysical Journal International, 152(1), 215–223.

Bormann, P. (Ed.) (2012). New Manual of Seismological Observatory Practice 2 (NMSOP-2), Chapter 3: Seismic Sources and Source Parameters (Eq. 3.118). IASPEI, GFZ German Research Centre for Geosciences, Potsdam.

Brune, J. N. (1970). Tectonic stress and the spectra of seismic shear waves from earthquakes. Journal of Geophysical Research, 75(26), 4997–5009.

Brune, J. N. (1971). Correction to "Tectonic stress and the spectra of seismic shear waves from earthquakes". Journal of Geophysical Research, 76(20), 5002.

Dreger, D. S. (1994). Investigation of source scaling using empirical Green's functions. Bulletin of the Seismological Society of America, 84(1), 91–103.

EarthScope Consortium (2026). FDSN Web Services — dataselect and station; broadband data of stations IU.KBL and GE.KBU.

Hanks, T. C., & Kanamori, H. (1979). A moment magnitude scale. Journal of Geophysical Research, 84(B5), 2348–2350.

Hartzell, S. H. (1978). Earthquake aftershocks as Green's functions. Geophysical Research Letters, 5(1), 1–4.

Kikuchi, M., & Kanamori, H. (1982). Inversion of complex body waves. Bulletin of the Seismological Society of America, 72(2), 491–506.

Konno, K., & Ohmachi, T. (1998). Ground-motion characteristics estimated from spectral ratio between horizontal and vertical components of microtremors. Bulletin of the Seismological Society of America, 88(1), 228–241.

Mueller, C. S. (1985). Source pulse enhancement by deconvolution of an empirical Green's function. Geophysical Research Letters, 12(1), 33–36.

Scordilis, E. M. (2006). Empirical global relations converting MS and mb to moment magnitude. Bulletin of the Seismological Society of America, 96(2), 484–494.

U.S. Geological Survey (2026). Earthquake Catalog, FDSN event web service (ComCat).

Wheeler, R. L., Herold, D. M., & Rukstales, K. S. (2005). Seismotectonic map of Afghanistan, with an annotated and digitized seismic catalog. U.S. Geological Survey Open-File Report 2005-1264.

Appendix A. Complete catalog of the 58 events

The complete research catalog with the converted Mw magnitudes is given in Table A1. The "Role" column identifies the accepted target events and the EGF events used; the "Agency" column is the organization that reported the catalog magnitude (all Mw values except the ML event with ID 636673972 were obtained from the Bormann-relation conversion).

Table A1. The 58-event catalog of the Sarobi region (2002–2024) with M_w magnitudes.

[Insert Table A1 here]

ISC ID	Date	Time (UTC)	Latitude (°N)	Longitude (°E)	Depth (km)	M_w	Agency	Role
3522931	2002-08-13	19:56	34.8800	69.9121	35.0	3.06	ISC	—
3518745	2002-10-15	00:31	34.7878	69.7616	35.0	3.34	ISC	—
6144016	2002-11-30	21:55	33.9707	69.4904	19.0	3.34	ISC	—
6542083	2003-01-23	01:32	36.0724	71.1427	100.0	3.34	ISC	—
7307672	2004-03-10	15:54	34.5309	69.5780	24.0	3.90	ISC	—
7398178	2004-09-05	01:30	33.9228	69.8588	35.0	3.76	ISC	—
8011815	2005-12-27	00:01	34.3860	69.5676	24.0	3.62	NEIC	—
8184462	2005-12-29	08:20	34.5223	69.2898	35.0	3.06	ISC	—
8079421	2006-01-27	18:58	34.5485	69.6990	45.0	4.45	ISC	—
8113501	2006-02-05	22:51	34.5337	69.6382	24.0	3.34	ISC	—
10388725	2007-01-18	10:18	34.5193	69.9234	63.0	3.76	ISC	—
13335548	2008-01-16	03:17	34.5743	69.7142	24.0	3.34	ISC	EGF
11158472	2008-05-09	13:50	34.4216	69.6455	24.0	2.93	ISC	—
13391904	2008-08-17	00:41	34.2351	69.5675	19.0	3.90	ISC	—
13391936	2008-08-17	14:02	34.0812	69.4179	19.0	3.76	ISC	—
13393824	2008-09-08	20:39	34.5929	69.5183	24.0	3.62	ISC	—
11377995	2008-09-24	09:07	34.3853	69.5794	24.0	3.20	ISC	—
12934544	2009-04-05	19:39	34.0503	69.8690	35.0	3.20	ISC	—
13439428	2009-05-08	22:47	34.2420	69.3288	24.0	3.34	ISC	—
13553117	2009-05-10	03:49	34.1253	69.9363	35.0	3.20	ISC	—
14876428	2010-05-15	13:31	34.3532	69.4577	24.0	3.06	ISC	EGF
15608636	2010-10-16	02:05	34.5958	69.4653	24.0	2.93	IDC	—
16587344	2011-06-01	03:43	34.3552	69.5031	24.0	3.62	ISC	—
16577383	2011-06-04	06:29	34.3773	69.3656	24.0	3.90	ISC	Target
16557032	2011-06-04	12:01	34.4792	69.4243	24.0	3.90	ISC	—
17324789	2011-09-25	12:21	34.4466	69.4124	24.0	4.45	ISC	Target
17386813	2011-10-19	13:31	34.5391	69.7238	24.0	4.04	ISC	Target
600099392	2011-12-14	23:03	34.3864	69.5044	24.0	3.20	ISC	—
600501552	2012-01-02	02:15	34.6871	69.6080	24.0	2.51	NNC	—
601022765	2012-05-18	12:45	34.3927	69.6442	24.0	4.59	ISC	Target
603176027	2013-06-20	23:23	34.0366	70.0161	35.0	3.06	ISC	—
604093297	2014-02-27	14:21	34.6574	69.6234	10.0	3.20	ISC	EGF
605324624	2014-09-18	21:32	34.4068	70.1905	35.0	3.90	ISC	—
606981536	2015-03-20	08:24	33.6950	69.3833	35.0	3.62	ISC	—
608498978	2016-02-13	08:01	34.3537	69.7173	24.0	3.20	ISC	EGF
608543546	2016-04-07	21:24	34.1994	69.7325	35.0	3.48	ISC	—
608898748	2016-05-20	01:40	34.7365	69.3290	35.0	3.34	ISC	—
615074949	2016-11-25	18:22	34.2849	69.6737	24.0	3.20	ISC	—
609835994	2016-12-08	10:02	34.2655	69.3524	24.0	4.18	ISC	—
610415472	2017-02-13	22:55	34.4949	69.6603	24.0	2.79	ISC	EGF
610588568	2017-04-29	06:17	34.3723	69.8820	35.0	3.76	ISC	—
610641851	2017-05-17	16:19	34.1731	69.3927	10.0	4.18	ISC	—
617428845	2019-09-04	05:53	34.4851	69.3452	24.0	3.20	ISC	—
618936064	2020-08-30	05:44	34.3119	69.5966	24.0	3.62	ISC	—
625783059	2021-05-19	09:19	34.7019	69.5439	24.0	4.45	ISC	—
624574960	2022-07-16	11:27	34.5861	69.7532	22.7	4.59	ISC	—

ISC ID	Date	Time (UTC)	Latitude (°N)	Longitude (°E)	Depth (km)	M_w	Agency	Role
624605874	2022-07-16	11:34	34.3175	69.7235	24.0	3.90	ISC	—
624749335	2022-09-04	21:57	34.6966	70.8251	10.9	5.57	ISC	—
625391591	2022-12-11	01:52	34.5912	69.5898	24.0	4.04	ISC	Target
625858695	2022-12-16	13:10	34.6045	69.5026	86.4	2.51	NNC	—
625550131	2022-12-24	15:05	34.3352	69.5419	35.0	2.93	ISC	—
626349400	2023-06-20	06:14	34.5519	69.5940	24.0	3.20	ISC	—
626329411	2023-06-25	15:49	34.5542	69.6560	10.0	4.32	ISC	Target
636673972	2023-08-28	06:03	37.7075	72.8012	10.0	3.50	NDI	—
626719142	2023-08-31	16:53	34.6745	69.5680	10.0	4.32	ISC	—
636757312	2024-02-09	03:21	34.6617	69.4511	24.0	3.34	ISC	—
637460170	2024-04-12	03:00	34.5182	69.5892	10.0	2.79	ISC	—
641557318	2024-05-27	17:56	34.4209	69.6929	24.0	3.06	ISC	—

Appendix B. Quality-control details of the accepted pairs

Table B1 reports the six quality criteria of the accepted pairs for the final band of each event: the correlation of the full window and of the onset pulse, the mean signal-to-noise ratio of the two events, the deviation of the spectral-ratio level from the moment anchor (in dex), and the flatness of the ratio at low frequencies (0.5–1.5 Hz).

Table B1. Detailed quality criteria of the six accepted pairs.

[Insert Table B1 here]

Target event	Band	cc (window)	cc (pulse)	SNR (target)	SNR (EGF)	Moment deviation (dex)	Flatness (dex)	QC
601022765	P	0.279	0.599	2305	219	0.51	0.189	6/6
17324789	S	0.541	0.685	10	5	1.88	0.203	4/6
626329411	P	0.278	0.574	2185	742	1.08	0.173	5/6
17386813	P	0.373	0.971	467	424	0.71	0.122	6/6
625391591	P	0.499	0.764	2053	964	0.93	0.143	5/6
16577383	P	0.374	0.669	291	165	0.83	0.232	5/6

QC: number of criteria accepted out of the six criteria of Table 2; moment deviation: $|\log_{10}(\Omega_{0r}) - 1.5 \cdot \Delta M_w|$.